An expansion of the binocular zone and interocular mismatch, arising from deletion of Ten-m3, induces the formation of ocular dominance domains in mouse visual cortex

Sam Merlin[1], Sam Horng[2], Lauren R. Marotte[3], Mriganka Sur[2], Atomu Sawatari[1] and Catherine A. Leamey[1]

1. Discipline of Physiology, School of Medical Sciences and the Bosch Institute, University of Sydney, NSW, 2006, Australia
2. Dept of Brain and Cognitive Sciences, MIT, Cambridge, MA, 02139, USA
3. Visual Sciences Group, Research School of Biology, ANU, Canberra, ACT, 0200, Australia

Corresponding author: Catherine A. Leamey

cathy@physiol.usyd.edu.au

Figures: 6

Tables: 0

Supplementary material: 2 figures

Text: 3986 words

Keywords: Primary visual cortex, ipsilateral mapping, binocular, Ten-m, Odz, ocular dominance, suppression.

Abstract:

The visual system contains precise retinotopic mapping of each eye onto central structures, together with exquisitely matched projections from the two eyes. Ten-m3, a transmembrane glycoprotein, acts as an eye-specific axonal guidance cue in the retinogeniculate pathway. Significantly, ipsilateral projections are not visuotopically aligned with contralateral projections in Ten-m3 knockout mice. Here, we demonstrate that subcortical mismapping of binocular input is conveyed to primary visual cortex (V1) in Ten-m3 knockouts: ipsilateral inputs are widely distributed across V1, rather than being restricted laterally as in controls, and are interdigitated with contralateral inputs into ocular dominance domains in V1. Furthermore, ipsilateral and contralateral inputs are mismatched at the level of single V1 neurons and binocular stimulation leads to functional suppression of these neurons. Thus, a medial expansion of the binocular zone together with an interocular mismatch is sufficient to induce novel structural features such as ocular dominance domains in rodent visual cortex.

A key organizing principle of the central nervous system is its topography. This is exemplified in the visual system, where the projection of the visual field onto the retina is mapped systematically onto the dorsal lateral geniculate nucleus (dLGN) and primary visual cortex (V1). There is compelling evidence that both intrinsic guidance mechanisms and activity-dependent processes play important roles in generating retinotopic maps in central structures[1-5].

In species with binocular vision, the generation of a cohesive map of the visual world requires the precise mapping of each retina onto central structures, as well as the alignment of the inputs from the two eyes that view the same region of space. In the dLGN these inputs remain segregated[6], but topographically appropriate[7, 8], and they come together in the binocular region of V1. In carnivorans and most primates geniculocortical inputs are largely segregated into ocular dominance columns in layer 4[9-13] of V1, whereas in rodent species no segregation is apparent. Rather, there is a single binocular zone which occupies approximately the lateral third of V1. The remaining, more medial parts are monocularly driven[14-16]. While there is strong evidence that activity-dependent processes during early development play important roles in determining the degree of drive provided to V1 by each eye[16-19], virtually nothing is known about how the inputs from the two eyes align with each other. Similarly, the rules that determine whether a given species will exhibit segregation of ocular drive in V1 are unclear.

We have recently reported that the transmembrane glycoprotein Ten-m3 plays a critical role in regulating the alignment of the inputs from the two eyes in the thalamus. In Ten-m3 knockout (KO) mice, ipsilateral inputs arise from the

ventrotemporal crescent, as in wildtypes (WTs) but are not confined to the normal binocular-encoding segment within the dorsomedial portion of the dLGN. Instead their terminations spread to the ventrolateral, normally monocular, region of the dLGN[20]. This change occurs in the absence of detectable changes in the topography of contralateral projections. Despite the altered ipsilateral mapping, eye-specific retinogeniculate inputs remain segregated. Behavioral analyses revealed that deletion of Ten-m3 is also associated with profound deficits in visual function, which remarkably, are reversed by acute monocular inactivation[20]. The unique phenotype of the Ten-m3 KO mouse, where there is a major expansion of the normally confined ipsilateral retinogeniculate projection, provides an excellent model to probe the mechanisms of binocular mapping and the impact of altered ipsilateral drive on the organization and function of V1.

Here, we utilize a number of complementary anatomical and functional approaches to show that the expansion and mismapping of ipsilateral inputs to the dLGN of Ten-m3 KO mice is conveyed to V1. This has a profound impact: it induces a novel ocular dominance structure and functional intracortical suppression of binocular responsiveness within V1.

Results

Ten-m3 deletion alters the distribution of ipsilateral drive in V1

We first addressed how the changes in the mapping of ipsilateral retinal axons in the dLGN affects the distribution of ipsilateral inputs to V1, using transneuronal tracing from one eye. In WT mice, contralateral inputs uniformly spanned the mediolateral extent of V1 (Fig 1a), whilst ipsilateral inputs were confined to lateral V1 (Fig 1b).

The patterning of contralateral projections to V1 in Ten-m3 KOs was largely similar to WTs (Fig 1c). The distribution of ipsilateral input was, however, dramatically different in KOs. Terminals were distributed across the much of the mediolateral extent of V1 (Fig. 1d), unlike WTs, where they were confined laterally. Thus, the percentage of ipsilateral labeling in the lateral-most third of V1 was significantly lower in KOs, but significantly higher in both middle and medial thirds (Fig. 1e; % label (mean ± s.e.m.): WT medial (0.97 ± 0.28), middle (24.43 ± 2.12) and lateral (76.34 ± 2.59); KO medial (12.45 ± 3.27), middle (52.57 ± 4.72) and lateral (35.20 ± 4.04); multivariate ANOVA, medial $F(1,22)=12.26$, $p=0.002$; middle $F(1,22)=29.567$ $p<0.001$; lateral $F(1, 22) = 73.63$, $p<0.001$; $N_{WT}=4$, $N_{KO}=4$). The significant medial-ward shift in the distribution of ipsilateral projections indicates that the aberrant ipsilateral retinal input previously observed in the dLGN[20] is transferred to V1 .

In addition to the change in the mediolateral extent of ipsilateral input, we observed evidence of terminal clustering in KOs (Fig. 1d). This contrasts with WTs, where a single patch of label in the lateral portion of V1 was consistently observed (Fig. 1b). KOs exhibited significantly more patches in medial and middle zones, with the trend reversed in the lateral-most region (Fig. 1f; number of patches (mean ± s.e.m.): WT medial (0.00 ± 0.00), middle (0.33 ± 0.14), and lateral (1.00 ± 0.00); KO medial (0.58 ± 0.15), middle (1.17 ± 0.17), and lateral (0.83 ± 0.11); multivariate ANOVA, medial: $F(1,22)=15.40$, $p=0.001$; middle: $F(1,22)=14.47$, $p=0.001$; lateral: $F(1,22)=2.200$, $p=0.152$; $N_{WT}=4$, $N_{KO}=4$). We also saw evidence for patches of reduced labeling in contralateral V1 of KOs (Fig 1c, arrow, clearly visible as a dip in the intensity plot), although they were less prominent than in the ipsilateral hemisphere. This lack of clarity is very likely due to “spill-over”of tracer, a limitation of this method which has

more impact in the contralateral than the ipsilateral hemisphere[21, 22]. This bias would be expected to be even more pronounced in mice given the very large dominance of the contralateral projection.

To determine whether the mismapped ipsilateral inputs are able to drive cortical neurons, we examined the expression of the product of the immediate early gene c-fos (a marker for neural activity) in acutely monocularly-inactivated mice. This revealed the extent of monocular drive to both cortical hemispheres (for monocular-inactivation experiments, laterality is given with respect to the active eye). In WTs, high levels of reactivity were distributed across much of the mediolateral extent of contralateral V1, predominantly in layer IV (Fig. 2a). In ipsilateral V1, c-fos immunoreactivity was confined to the lateral region, with little or no staining in medial V1 (Fig. 2b), consistent with the pattern of transneuronal labeling. In contrast, Ten-m3 KOs exhibited patches of c-fos reactivity distributed across much of the mediolateral extent of ipsilateral V1 (Fig. 2d). Activity was consistently high across much of contralateral V1in KOs, however, patches of low reactivity, mirroring the patches of high reactivity seen in the other hemisphere, were also frequently observed (Fig. 2c). The patchy distribution seen with both c-fos staining and transneuronal tracing suggested that the medial expansion of ipsilateral mapping may induce a novel ocular dominance structure.

To examine this possibility, tangential sections through layer IV from monocularly-inactivated mice were used to determine the pattern of monocular cortical drive across the extent of V1. In all WTs ($N_{WT} = 6$) high reactivity was present across contralateral V1 (Fig 2e), and in a single, large patch in the lateral region of ipsilateral

V1 (Fig 2f). A strikingly different distribution was observed in ipsilateral V1 of Ten-m3 KOs, where clusters of highly immunoreactive neurons were aggregated in bands, 300-350μm wide, which traversed much of V1 (Fig 2h) interdigitated with regions of very low immunoreactivity (Fig 2h). While clusters encroaching onto medial V1 were observed in all KOs ($N_{KO} = 6$), the pattern of staining varied between cases (Supplementary Fig 1). Activity was generally high in contralateral V1, though similar patches of low reactivity, presumably revealing ipsilaterally-dominated domains, were also observed (Fig 2g). Quantification confirmed these changes. In KOs staining was significantly reduced in lateral V1 and increased in middle V1 with a non-significant increase for medial V1 (Fig 2i; % label (mean ± s.e.m.): WT medial (7.78 ± 1.40), middle (30.08 ± 1.66) and lateral (62.14 ± 2.80); KO medial (10.92 ± 1.327), middle (42.50 ± 2.91) and lateral (46.58 ± 3.29); multivariate ANOVA, medial $F(1,10)= 2.65$, $p=0.135$; middle $F(1,10)= 13.76$, $p=0.004$; lateral $F(1,10)= 12.99$, $p=0.005$). KO mice also showed a significant increase in the number of patches of c-fos reactive regions in medial and middle V1 (Fig 2j; number of patches (mean ± s.e.m.): WT medial (0.00 ± 0.00), middle (0.83 ± 0.17), and lateral (1.00 ± 0.00); KO medial (0.67 ± 0.21), middle (2.67 ± 0.33), and lateral (2.00 ± 0.58); multivariate ANOVA, medial: $F(1,10)= 10.00$, $p=0.010$; middle: $F(1,10)= 24.20$, $p=0.001$; lateral: $F(1,10)= 3.00$, $p=0.114$). The patchy, medially-shifted distribution of c-fos expression provides further evidence for the novel emergence of eye-specific domains due to aberrant ipsilateral drive within V1 of Ten-m3 KOs. Interestingly, the clustering observed with c-fos staining was more punctate than seen with transneuronal tracing. This may reflect technical limitations of the transneuronal technique, mentioned above. Alternately, intracortical mechanisms may result in an accentuation of the functional segregation beyond that which is present anatomically.

Deletion of Ten-m3 causes no change in receptive field properties and retinotopy of the contralateral projection

Our anatomical data lead to predictions regarding cortical activation: (1) single V1 neurons may receive inputs from disparate parts of the visual field via the ipsilateral and contralateral eyes; (2) the formation of eye-specific domains may increase the degree to which cells are dominated by a single eye; and (3) the visuotopically misaligned projections may influence binocular compared to monocular responses of V1 neurons. To test these hypotheses, single-unit recordings and intrinsic signal optical imaging in anesthetized mice were performed. For quantitative analysis of single-unit data, sampling was restricted to lateral V1, the only region that usually receives binocular input, so WT data could form an appropriate control. For comparison, a few cells recorded from more medial V1 are described qualitatively.

Firing rates showed no difference between WT and KO during stimulation of the contralateral eye ((mean ± s.e.m.): KO contra (n = 34): 21.48 ± 3.23 spikes/s; WT contra (n = 36): 23.16 ± 2.77 spikes/s; Mann-Whitney U-test: U = 1153, p = 0.53). A reduction in firing rate was observed in KOs during stimulation of the ipsilateral eye compared to WT (KO ipsi (n = 34): 8.53 ± 1.39; WT ipsi (n = 36): 16.91 ± 2.67; Mann-Whitney U-test: U = 997, p = 0.014). This is consistent with the reduced ipsilateral drive in lateral V1 in Ten-m3 KOs. RF size showed no difference between WT and KO for either eye (Fig 3a; KO contra: 16.2 ± 0.7^{o}; WT contra: 17.5 ± 0.8^{o}; KO ipsi: 15.6 ± 1.1^{o}; WT ipsi: 16.0 ± 0.6$^{o;}$ N_{WT} = 24, N_{KO} =32; ANOVA F(3, 94) = 0.78, p = 0.509). The location of the centers of contralateral RFs in lateral V1 did not

differ from WT for either the azimuth or elevation axes (mean ± sem: azimuth WT 19.77 ± 3.11°, KO 17.49 ± 3.89°; Mann-Whitney U-test, U= 773, p=0.98; elevation WT 7.87 ± 1.82 °, KO 17.46 ± 3.89 °; Mann-Whiney U-test, U=731, p = 0.47; N_{WT} = 25 cells, N_{KO} = 36 cells). Recordings from more medial V1 showed the expected retinotopic shift towards more peripheral visual field for both WTs and Ten-m3 KOs (Supplementary Fig 2).

Individual V1 neurons receive inputs from disparate parts of the visual space in Ten-m3 KOs

In WT mice the ipsilateral and contralateral RFs were typically overlapping (Fig 3c, top) and their mean center-to-center separation, 9.5 ± 2.2° (median 0°) of visual space (Fig 3b), was smaller than the mean RF diameter obtained here (Fig. 3a) and previously reported in mice (10 - 20°)[15, 23, 24]. This was not the case for Ten-m3 KOs where the mean separation of RFs, 25.9 ± 3.7° (median 18.0°) was almost 3-fold greater than in WTs (Fig 3c bottom, Fig 3b; Mann-Whitney U-test, U = 493, p = 0.001; N_{WT} = 25 cells, N_{KO} = 32; 4 KO cells received exclusively monocular input and were excluded from this analysis). The marked increase in the separation of RFs, in the absence of change in RF size, means that ipsilateral and contralateral RFs are typically not overlapping in Ten-m3 KOs.

Our anatomical data predict that medial V1 will also receive ipsilateral drive in Ten-m3 KOs. This was found to be the case, with medially-situated V1 cells receiving ipsilateral and contralateral input from disparate regions of the visual field (2 cells; Supplementary Fig 2). Recordings from a similar region of V1 in WTs did not exhibit ipsilateral drive (6 cells).

Deletion of Ten-m3 drives the formation of functional ocular dominance domains in V1

We next asked whether the altered ipsilateral mapping alters the ocular dominance index (ODI) of Ten-m3 KO mice (ODIs of 1 and -1 indicate entirely contralateral or ipsilateral drive, respectively; see Methods). While the mean ODI was not significantly different between KOs and WTs based on this sample, there was evidence that the KO values were more widely distributed, including examples of cells with entirely contralateral drive (n = 2) and entirely ipsilateral drive (n = 2; Fig 3d). No WT cells exhibited entirely monocular drive. The presence of even a fairly small (circa 10% total cells) number of entirely, and very strongly, ipsilaterally-dominated cells in Ten-m3 KOs is a striking finding: to our knowledge, no previous study has reported the presence of entirely ipsilaterally-driven cells in rodents using single-unit electrophysiological recording in the absence of a visual manipulation such as monocular deprivation. In order to assess the level of ocular dominance independent of the eye, the absolute value of the ODI, or monocularity index (MI) was calculated. The mean MI is significantly higher in KOs than WTs (Fig 3e inset; WT (mean ± s.e.m.): 0.27 ± 0.05 (median: 0.22); KO (mean ± s.e.m.): 0.54 ± 0.05 (median: 0.53); $N_{WT} = 24$, $N_{KO} = 36$; Mann-Whitney U-test, U = 508, $p<0.001$). The significant rightward shift of the MI cumulative probability function for Ten-m3 KOs is consistent with an increase in monocularity (Fig 3e; Kolmogorov-Smirnov test, D = 0.44, p = 0.004).

Intrinsic signal optical imaging in response to monocular stimulation was used to examine whether or not there were novel ocular dominance domains in Ten-m3 KOs,

as suggested by the anatomical and single-unit data. In WTs, a single, large domain receiving a moderate degree of ipsilateral drive was confined to the lateral region of V1, whereas contralateral drive was relatively uniform across V1. In Ten-m3 KOs, domains which received little or no contralateral drive were present. These regions received very strong ipsilateral drive (Fig 4a). The overall ODI showed a significant shift towards the ipsilateral eye in Ten-m3 KOs for the azimuth axis (when a bar drifting periodically in the azimuth dimension was used to stimulate the visual field) and a non-significant trend for the elevation axis (Fig 4b; (mean ODI ± s.e.m.) azimuth: WT = 0.35 ± 0.08, KO = 0.02 ± 0.04, Student's t-test, $p<0.001$, $N_{KO} = 5$, $N_{WT} = 7$; elevation: WT = 0.25 ± 0.10, KO = 0.08 ± 0.08, Student's t-test, $p=0.34$, $N_{KO} = 5$, $N_{WT} = 5$). The region of V1 receiving ipsilateral input was also enlarged in KOs, with ipsilaterally-dominated regions extending significantly more medially in Ten-m3 KOs (Fig 4c; (mean number of ipsilateral-driven patches ± s.e.m.) WT: medial (0.0 ± 0.0), middle (0.7 ± 0.15), lateral (1.0 ± 0.0); KO: medial (0.25 ± 0.16), middle (1.62 ± 0.18), lateral (1.12 ± 0.12); Multivariate ANOVA medial $F = 2.96(1, 16)$, $p=0.104$; middle $F = 15.31(1, 16)$, $p=0.001$; lateral $F = 0.07 (1, 16)$, $p=0.276$).

Mismapped ipsilateral input contributes to suppression of binocular activity in V1

We previously reported that Ten-m3 KOs have severe deficits in performance of visual behavioural tasks when using both eyes which were rescued by monocular inactivation[20]. It is possible that the mismapped ipsilateral input in these animals leads to suppression of cortical activity during binocular stimulation. To investigate this, we used c-fos immunoreactivity to compare cortical activation levels in WTs and KOs following binocular viewing. In WTs ($N_{WT} = 3$), both hemispheres displayed

high levels of c-fos staining across layer IV (Fig 5a,b), suggesting ubiquitous activation during normal viewing conditions. In contrast, KO mice ($N_{KO} = 3$) exhibited markedly lower activity levels (Fig 5c,d). Tangential sections through layer IV confirm the consistency of this result across V1 (Fig 5e,f); these differences were significant (Fig 5g; (mean intensity ± s.e.m.) WT: 40.98 ± 1.87, KO: 23.27 ± 5.64, mixed-model ANOVA; $F(1,4) = 8.21$, $p = 0.046$). The activity levels observed in Ten-m3 KOs during binocular viewing were markedly lower than those observed in the hemisphere contralateral to the active eye during monocular viewing (Fig 2); no such difference was observed for WT. Quantification confirmed that monocular inactivation restored activity to WT levels (Fig. 5g; $WT_{monocular}$: 38.48 ± 1.79; KO monocular: 42.89 ± 1.96; ANOVA between-group comparison of label intensity, $F(3,56)= 26.574$, $p < 0.001$; $KO_{binocular}$ significantly different to all other groups ($KO_{monocular}$, $WT_{monocular}$ and $WT_{binocular}$), Tukey HSD post-Hoc; $p<0.001$ for all comparisons). These data provide evidence for a global suppression of V1 activity during binocular viewing in KOs which is fully rescued in the contralateral hemisphere by acute monocular inactivation.

To assess the possibility that misaligned interocular drive induces suppression at the level of single neurons, we compared firing rates of single-units in lateral V1 of WTs and KOs during contralateral monocular and binocular stimulation. We found that in 27% of KO neurons (6/22), firing levels were reduced during binocular versus contralateral monocular stimulation (Fig 5i; bottom). This was significantly different from WTs where no cells (0/22) exhibited suppression during binocular stimulation ($p=0.011$, Fisher's exact test). In WTs, the majority (>2/3) of cells were facilitated by binocular stimulation (Fig 5i; top) and the remainder displayed no change (Fig 5h).

While facilitation was observed in some Ten-m3 KO cells, this was less frequent than in WT (Fig 5h). Although seen in only a minority of cells, the significant increase in suppression under binocular conditions in Ten-m3 KOs is consistent with the behavioural phenotype[20] and c-fos data.

Discussion

Our data demonstrate that ipsilateral inputs to V1 are markedly expanded and mismatched with respect to contralateral inputs in Ten-m3 KO mice. This is associated with the emergence of an ocular dominance structure and functional suppression during binocular stimulation. The mapping changes are summarized in figure 6.

We propose that the emergence of eye-specific cortical regions in the Ten-m3 KO can be attributed to the mismapping of ipsilateral inputs to V1 which occurs as a consequence of inappropriate ipsilateral mapping in the thalamus (Fig. 6). This results in both a medial expansion of the binocular zone and misaligned ipsilateral and contralateral inputs, and drives the formation of eye-specific regions, presumably via activity-dependent processes. The enhanced inhibition associated with mismatched interocular inputs, together with an expanded binocular zone, provides a potential mechanism by which ocular dominance columns form in V1.

Both activity-dependent and independent mechanisms have been reported to contribute to the formation of eye-specific domains in carnivorans and primates. Pharmacological blockade of all retinal activity disrupts ocular dominance structure in

cats[22]. Visually-driven activity, however, is not required[22, 25, 26], although the misalignment of the inputs from the two eyes, as in strabismus, can increase the degree of monocularity in cats[12, 27]. The induction of binocular innervation of a single tectum in non-mammalian vertebrates can also cause segregation via activity-dependent processes[28-31]. These findings suggest that the spatial and/or or temporal decoupling of input from the two eyes can yield cortical eye-specific domains. In Ten-m3 KOs, the separation of the ipsilateral and contralateral RFs is greater than mean RF diameter. Further, the appearance of ocular dominance domains frequently resembles islands or patches. Interestingly, the appearance of ocular dominance columns representing the far peripheral field in primates, where RFs are larger (similar in size to those in rodents) also have this appearance[32]. The appearance of the ipsilaterally-dominated regions that are first seen at around 2 weeks postnatally (which is prior to eye-opening) in cat V1 also appear as isolated patches, surrounded by contralaterally-dominated regions[25]. It isseems likely, therefore, that the misalignment of visual drive from the two eyes in Ten-m3 KOs gives rise to their segregation via activity-dependent processes. Future studies should address whether eye-specific domains are present in V1of Ten-m3 KOs at eye-opening, which would implicate a role for spontaneous retinal activity[3], or whether visual experience is required to drive their formation.

The proportion of V1 receiving binocular inputs may be a determining factor for eye-specific segregation. There is an association between the number of ipsilaterally-projecting cells (which correlates tightly with eye-position and the size of the binocular field), and the proportion of V1 devoted to processing binocular inputs, with the presence (or absence) of ocular dominance columns[33]. In Ten-m3 KO mice, the

size and location of the origin of the ipsilateral projection[20], and thus size of the binocular field, are not altered. The proportion of V1 which receives binocular input is, however, greatly increased in Ten-m3 KOs. Computational models of columnar organization in cortex rely both on the magnitude of lateral excitation/inhibition and size of the mapped region relative to lateral interactions to generate feature-specific segregation[34, 35]. Indeed, modeling studies explicitly predict that, in the presence of inhibition, a large enough region dominated by one eye must break up to allow emergence of the other eye's inputs[36]. Thus, in Ten-m3 KO mice, both the expanded binocular zone and enhanced interocular suppression are probable mechanisms underlying ocular dominance column formation.

It has been suggested that the anatomical basis of ocular segregation is present from relatively early stages of development, just after thalamic axons invade layer IV[37, 38]. This specificity has been hypothesized to rely on cues which enable molecular matching of geniculocortical axons arising from the ipsilateral and contralateral recipient layers of the dLGN to specific subdomains of V1, which are independent of the eyes[37, 38]. Although our data do not specifically address this issue, it seems unlikely that the deletion of Ten-m3 would induce the expression of molecular matching cues in the geniculocortical pathway. Our data therefore suggest that, at least in mice, the molecular matching between ipsilateral and contralateral regions of the dLGN and V1 is not required for the formation of eye-specific cortical domains. This of course does not exclude the possibility that such cues may be present in other species and may account for the more regular distribution of ocular dominance domains seen in cats and primates.

Deletion of Ten-m3 may, however, exert more subtle alterations within V1, or between dLGN and V1, which could contribute to eye-specific segregation. Ten-m3 is a homophilic transmembrane glycoprotein[39, 40] which is expressed in corresponding topographically gradients in retina, dLGN and V1[20, 41], and has been identified as a potential downstream target of *Emx2*[42], a transcription factor which specifies caudal cortical areas[43, 44]. While shifted medially in Ten-m3 KOs (SHH and MS, unpublished data), V1 appears largely normal with lamination[20], geniculocortical topography, contralateral retinotopy, and response properties such as RF size remaining unchanged, suggesting that Ten-m3 exerts a relatively minor direct influence on these aspects of cortical development. In addition to any direct roles Ten-m3 may play in cortical development, the mismapped activity itself may also induce changes within V1 or connectivity between V1 and other areas. Alterations in the distribution of callosal projections, for example, have been reported in Siamese cats[45] where defects in decussation at the optic chiasm affect the mapping of ipsilateral inputs and can also cause cortical suppression[46-48]. These possibilities are the subject of ongoing investigation.

While present in Ten-m3 KOs, the functional suppression observed during recordings in V1 was less widespread than predicted by the binocular c-fos or the behavioural[20] data. Interestingly, the c-fos and behavioral data both reflect activity levels in awake-behaving animals, whereas the electrophysiological data is obtained in anesthetized preparations. It is possible that the more restricted suppression observed in the single-unit data may be due to the effects of anesthetic on V1 responsiveness. This could occur directly and/or via influences on top-down processing mechanisms associated with conscious visual perception. Additionally, the fact that only a portion of the

mouse's large visual field (~90° of 320^{o}) is stimulated during our single-unit recordings, and the confinement of our recordings to lateral V1 (which may minimize the effect of the mapping defect), could also reduce the level of suppression observed in this data. The source of the suppression, in particular whether it is intrinsic to V1 or is driven by other, potentially higher-order, cortical areas remains to be determined.

Methods

All experiments were performed in mice and approved by the University of Sydney Animal Ethics Committee and/or MIT's Committee on Animal Care and followed NIH and NHMRC guidelines. The Ten-m3$^{-/-}$ (KO) strain is maintained on a Black6/Sv129 cross; a mixed background is essential for the survival of the KOs (Leamey et al., 2007). Animals were obtained from heterozygote matings. WT littermates (Ten-m3$^{+/+}$) were used as controls. Only pigmented animals were used in this study. Genotyping was performed by PCR from tail biopsy.

Transneuronal tracing and autoradiography. Adult mice were anesthetized by inhalation of 2-4% isoflurane in oxygen. A monocular intravitreal injection of 150µCi of tritiated proline (Amersham) was made using a Hamilton syringe. Mice were euthanized 7 days later by an overdose of sodium pentobarbitone (50mg/kg), and perfused with 0.9% saline followed by 4% paraformaldehyde in 0.1M phosphate buffer (PB, pH 7.4). Brains were post-fixed overnight, cryoprotected and 40µm thick coronal frozen sections were prepared and mounted on acid-cleaned slides. Slides were dipped in NTB-2 emulsion (Kodak) and stored in darkness for 8-12 weeks. Slides were then developed in D-19 developer (Kodak), fixed and coverslipped. Images were captured using an AxioCam digital camera under darkfield illumination through a 5x objective and merged using Adobe Photoshop. Signal intensity was thresholded using Image J (NIH). For quantification, the visual cortex was divided into three equal parasagittal subdivisions: medial, middle and lateral thirds. The pixel density across layer IV was measured using Image J, and background signal was calculated from layer IV of a non-visual cortical area, and subtracted. The proportion of total label contained within each third was determined. The number of patches was

determined based on accumulations of label separated by low levels of label by two independent observers. Three V1 sections were from each of 4 WTs and 4 KOs were used for the quantification.

Immunoreactivity for c-fos. Mice were anesthetized as above and 1uL of 2μM tetrodotoxin (TTX; Sigma) was injected into the posterior chamber of the eye. Following recovery, animals were placed in a darkened room for 16-20 hours, prior to a 2 hour exposure to a novel, light environment. They were immediately euthanized and perfused as above. For binocular simulation the TTX injection step was omitted. For tangential sections, 2% paraformaldehyde was used and the cortices were removed and flattened between glass slides prior to post-fixation in 4% paraformaldehyde. Coronal or tangential sections were cut at 40μm on a freezing microtome. Sections were quenched prior to incubation overnight in α-c-fos antibody (1:5000; Santa Cruz). Reaction product was visualised with a biotinylated secondary antibody followed by incubation in ABC kit (Vector) and a diaminobenzidine reaction. Sections were coverslipped and photographed under brightfield illumination using an Olympus digital camera. Image J (NIH) was used to subtract background and threshold images. Threshold values were conserved for all sections from each animal. Level of immunoreactivity was calculated based on the amount of labeled pixels within layer IV of each animal.

Intrinsic optical imaging. Animals at age P28-P35 from Ten-m3 WT and Ten-m3 KO groups were anesthetized with 10% urethane (1.5 mg/g i.p.) and 1% chlorprothixene (0.2 mg/animal, i.p.). After the skull was exposed over the area of V1 and the animal was fixed in a custom-made stereotaxic frame, the region of interest

was covered with a 1.5% agarose solution and glass coverslip. The cortical surface was illuminated with a tungsten halogen light source and imaged with a custom built system with a CCD camera (Cascade 512B, Roper Scientific). Green light (550 nm) was used to obtain a reference image of the cortical vasculature at the surface, while red light (630 nm) was used for acquisition of intrinsic hemodynamic signals, focusing 300-500μm below the cortical surface. In a 62 x 72^0 region of visual space, a drifting horizontal or vertical white bar (9 s/cycle) over a uniformly gray background was presented to both eyes, as well as to the contralateral and ipsilateral eye alone. Images of V1 were captured at 15 frames/s for a stimulus session of 25 min. A temporal high pass filter (135 frames) was used to remove slow noise components. A temporal Fast Fourier Transform (FFT) component at the stimulus frequency (9 s^{-1}) was calculated pixel by pixel from the set of images[49]. To calculate the magnitude of response, the amplitude of the FFT component normalized to that of background in the absence of visual stimuli was measured and the average of the top 2000 pixels in the map was obtained. Retinotopic maps were generated from the phase of the FFT of the response time series at the stimulus frequency. To measure the size of the cortical area of stimulation, the magnitude map was filtered by thresholding at a level of 40% of the peak response and number of pixels measured within a defined area of interest. Ocular dominance values were calculated using the ocular dominance index (ODI), which takes the difference in magnitude of the contralateral and ipsilateral stimulated maps divided by the sum of the magnitudes; a value of -1 represents predominant ipsilateral drive while a value of +1 represents predominant contralateral drive.

Single-unit *in vivo* electrophysiology: Mice were anaesthetized with 1.2-1.5 mg/kg intraperitoneal injection of urethane, and placed in a modified stereotax (Kopf Instruments). Recordings were made using resin coated tungsten electrodes (~1MΩ at 1kHz; FHC, Bowdoin,ME), mounted in a headstage (Digitimer, Hertfordshire, UK) attached to a micromanipulator (Exfo-Burleigh, Quebec, Canada). Signals were amplified and band pass filtered (600 to 4000Hz) using a NeuroLog amplifier (Digitimer, Hertfordshire, UK). Waveforms were captured using manually determined thresholds and stored to disk using EXPO (EXPO developed by Peter Lennie, University of Rochester).

Visual Stimuli: Computer generated stimuli (EXPO) were projected via an LCD projector (EMP-TW700, Epson) onto a matt white, fixed front projection screen (1700 x 1270mm; 2130mm diagonal) placed 75 cm in front of the animal. Receptive fields (RF) for each eye were mapped using a square stimulus of 10° x 10^{o} visual angle presented (for a duration of 250ms every 500ms) pseudo-randomly throughout extent of the visual field (over 500 presentations total). Averaged RF maps were generated using custom software (Matlab). RF sizes were estimated by thresholding maps, and then back-converting the pixel counts to angle of visual degrees in both x and y dimensions. Similarly, ipsilateral and contralateral RF separation was determined by calculating the linear distance between the peaks of eye specific RF maps and back-converting pixel distances to degrees of visual extent. The ocular dominance index (ODI) was calculated as follows: ODI = (C – I)/(C + I). C and I correspond to the mean response to stimulation of the contralateral eye and ipsilateral eye respectively. A second measurement, the monocularity index (MI; MI = |ODI|) was used to determine ocular dominance independent of the eye.

Stimulus for binocular and monocular responses consisted of a full field, drifting sinusoidal grating (drift rate: 2cycle/^{o}, spatial freq 0.03 cycle/ ^{o}, orientation: 0^{o}) presented for one second every two seconds for 40 iterations. A sequence of contralateral monocular – binocular – contralateral monocular visual stimulation was used on each subject. Cells were considered to exhibit suppression or facilitation only if their mean binocular response was less or greater than their response to both blocks of monocular activation.

Statistical Analysis

Statistical analysis was performed using Excel, Matlab, and SPSS, using Student's t-test, Mann-Whitney U-test, ANOVA, Kolmogorov-Smirnov test and Fishers exact test as indicated in the results.

ACKNOWLEDGEMENTS

This work was supported by an NHMRC project grant and University of Sydney research and development grant to CAL, and NIH grants EY017098 and EY007023 and a grant from the Simons Foundation to MS.

AUTHOR CONTRIBUTIONS

SM performed anatomical tracing, c-fos staining and single-unit recording experiments. SH performed optical imaging experiments. LRM contributed to transneuronal tracing experiments. AS performed single-unit recordings. SM, SH and AS analyzed data. CAL, AS, MS and SM designed experiments. CAL, AS and SM wrote the paper.

Figure Legends

Figure 1 Ipsilateral inputs to V1 invade medial, normally monocular, regions of V1 in Ten-m3 KOs.

a-d: Contralateral (a,c) and ipsilateral (b,d) coronal sections through V1 from WT. WT **(a,b)** and Ten-m3 knockout mice **(c,d)** following transneuronal transport of tritiated proline from the eye. Plots below each photomicrograph plot relative signal intensity across layer IV to highlight fluctuations. Label in the contralateral cortex of WTs **(a)** is uniformly distributed across the medial to lateral extent of layer IV. Ipsilateral labeling in WTs was restricted to the lateral region of V1 **(b).** In Ten-m3 KOs, labeling in contralateral V1 is largely uniform, although areas of reduced density are also visible **(c, arrow)**. In Ten-m3 KO mice, label in ipsilateral V1 is not confined to lateral V1, but rather is distributed over much of the mediolateral extent of V1 **(d)**. Label is aggregated into clusters (arrows). Boundaries of V1 marked by arrowheads. Scalebar: 500μm, applies to all images.

e: Quantification of the proportion of transneuronal label present in the medial, middle, and lateral thirds of ipsilateral V1 as a percentage of total V1 label. Ten-m3 knockout mice showed a significant reduction in lateral label, and significant increases in middle and medial transneuronal label. Data based on 3 sections from each of 4 WT and 4 KO mice (mean ± sem).

f: Quantification of the number of patches of transneuronal label in medial, middle and lateral divisions of ipsilateral V1. Ten-m3 knockout mice showed less patches in lateral V1, and significantly more patches in central V1 (mean ± sem).

* $p<0.05$, ** $p<0.01$, *** $p<0.001$; Multivariate ANOVA, see results for details.

Figure 2 Altered pattern of ipsilateral drive in V1 as demonstrated using c-fos immunoreactivity.

a-d: Coronal sections through visual cortex of monocularly inactivated WT (**a,b**) and Ten-m3 KOs (**c,d**). Contralateral to the active eye uniformly high levels of reactivity are seen in WT **(a)**. Ipsilateral to the active eye high levels of reactivity are restricted to lateral V1 **(b).** In Ten-m3 KOs patches of low reactivity (arrows) are visible within the generally high staining within contralateral V1 **(c)**. Ipsilateral to the active eye, patches of high reactivity (arrows) are scattered across the entire medial to lateral extent of V1 **(d)**. Arrowheads mark V1 boundaries. Scale in a: 500μm, applies to a-d. M: Medial, L: Lateral.

e-h: Tangential sections through layer IV of monocularly inactivated wildtype **(e,f)** and knockout mice **(g,h)**, contralateral **(e,g)** and ipsilateral **(f,h)** to the active eye. In WTs uniformly high imunoreactivity is seen across contralateral V1 (**e**), whereas in the ipsilateral hemisphere it is confined to lateral V1 (**f, medial border of binocular region highlighted by dotted white line**). In Ten-m3 KOs, staining is mostly high in contralateral V1, although patches of very low reactivity are also seen **(g, *)**. In the ipsilateral hemisphere, intense staining is not restricted to lateral V1 and comprises distinct bands of high reactivity (*) which are separated by bands of low reactivity **(h)**. Dashed lines mark V1 borders. Scale in e: 500μm, applies to e-h.

i: Percentage of label in medial, middle and lateral thirds of ipsilateral V1. Significant changes in the distribution of ipsilateral label are observed in Ten-m3 KOs (mean ± sem).

j: Ten-m3 knockout mice show significant increases in the number of ipsilaterally-driven patches in medial and middle thirds of V1 (mean ± sem).

* $p<0.05$, ** $p<0.01$; Multivariate ANOVA, see results for details.

Figure 3 Increased separation of contralateral and ipsilateral drive in Ten-m3 KOs.

a: Graph plotting mean receptive field (RF) size for the contralateral and ipsilateral eyes (mean ± sem). No difference is observed between WT and Ten-m3 KO (ANOVA $F(3, 94) = 0.778$, $p = 0.509$).

b: Population differences in contralateral and ipsilateral drive separation between WT ($n = 25$) and KO ($n = 32$) V1 units. KO receptive fields have significantly greater separation compared to WT (Mean $\pm$ sem). WT: 9.5 ± 2.2^{o} (median 0^{o}); KO: 25.9 ± 3.7^{o} (median 18.0^{o}); Mann-Whitney U test, $p<0.01$.

c: Sample normalized receptive field 'heat' maps (see Methods) recorded from lateral area 17 of WT (top row) and Ten-m3 KO mice (bottom row) during stimulation of the contralateral (left) and ipsilateral (centre) eyes. Overlay maps of activity from both eyes (right) show far greater separation of ipsilateral and contralateral drive in Ten-m3 KOs. The vertical meridian is shown as a white line, dotted lines mark 10^{0} on either side.

d: Histogram plotting percentage of cells with a given ocular dominance index (ODI; 1= contralateral only, 0= equal ipsilateral and contralateral drive, -1= ipsilateral only) in WTs (black, top) and Ten-m3 KOs (bottom, grey). Note the presence of a subset of entirely ipsilaterally-driven cells in Ten-m3 KOs.

e: Cumulative probability distribution function of monocularity index (MI) shows a shift to the right indicating a significant increase in monocularity in Ten-m3 KOs. This is also reflected in the mean MI (inset).

Figure 4 Optical imaging of intrinsic hemodynamic signals demonstrates increased segregation of eye-specific domains in V1 of Ten-m3 KO mice.

a: Contralateral ("Contra") and ipsilateral ("Ipsi") driven maps are displayed along with a map of ocular dominance index (ODI) values. ODI is a measure of the relative eye-specific drive of each pixel, as calculated by the difference in response magnitudes from the contralateral and ipsilateral driven maps divided by the sum. Segregated regions (white arrows) of strong ipsilateral (blue) and contralateral (red) drive are detected in Ten-m3 KO mice. Ipsilateral regions extend more medially than the typical binocular zone of the wild-type. The ipsilaterally responsive region is outlined in dotted blue in the "Ipsi" panel and black in the "ODI" panel. Scale bar=500 μm, A=anterior, L=lateral. The bar shows the fractional change in reflection in greyscale. The area displayed is a visual approximation of the response amplitude of the activated region thresholded to a level of 30% of the peak response. The colorbar represents the ODI value; Blue (-1) indicates predominate ipsilateral drive while red (+1) represents predominant contralateral drive.

b: In the azimuth maps, the average ODI value of the ipsilaterally driven region is significantly decreased in the Ten-m3 KO mouse (indicating more ipsilateral drive, ** $p<0.001$). In the elevation maps, the average ODI value of the ipsilaterally driven region shows no statistically significant difference although there is a trend of decrease in Ten-m3 KOs (mean ± sem).

c: Measurement of the number of ipsilateral territories within the medial, middle and lateral thirds of V1 show that ipsilateral input is shaped into patches that project more medially in Ten-m3 KOs than in WTs (* $p=0.001$; mean ± sem).

Figure 5 Binocular stimulation induces suppression in V1.

a-d: Coronal sections through visual cortex of WT (**a,b**) and Ten-m3 KO (**c,d**) mice following binocular stimulation. WT mice display uniformly high levels of c-fos reactivity across both hemispheres whereas much lower levels of staining are seen in KOs. Arrowheads mark V1 boundaries. Scale in a: 500μm, applies to a-f. M: Medial, L: Lateral.

e,f: Tangential sections through layer IV of V1 in WT (e) and Ten-m3 KO (f) show markedly reduced activity across the whole of V1.

g: Quantification of c-fos immunoreactivity in WT and KO mice following binocular and monocular stimulation. Pixel density (mean ± sem) was significantly higher across the whole of V1 in WTs versus Ten-m3 KOs under binocular viewing, but this was rescued under monocular viewing, with WT and KO immunoreactivity at similar levels. * $p<0.05$, see results for details.

h: Graph showing proportion of cells that were facilitated (F), showed no change (N) or were suppressed in WTs and Ten-m3 KOs. In WTs over 2/3 of cells were facilitated and the remainder showed no change during binocular versus contralateral monocular stimulation; no WT cells showed suppression. In KOs, there was a significant increase in the proportion of cells which showed suppression and the number of facilitated cells was reduced.

i: Post-stimulus time histograms showing responses from a typical WT cell and an example of a KO cell exhibiting suppression during binocular stimulation. Graphs plot activity during contralateral monocular stimulation (Monoc, left), binocular stimulation (Binoc, middle) and a return to contralateral monocular stimulation (right). Firing rate increased or stayed constant under binocular stimulation compared to contralateral monocular stimulation in WT whereas it decreased in the KO (6 of 22

cells showed this pattern in KO, compared to 0 of 22 cells in WT, $p<0.05$, Fisher's exact test).

Figure 6

Schematic diagram showing normal mapping of the right visual field onto the retinogeniculocortical pathway in WT mice (left) and changes in Ten-m3 KOs (right). In WTs, the central, binocular field (purple) is viewed by the ventrotemporal region of both retinae. Contralaterally projecting retinal axons from the right temporal retina (blue) and ipsilaterally-projecting axons from the left temporal retina (red) target the dorsomedial segment of the dLGN. More nasal parts of the retina view more peripheral parts of the visual field which are not seen by the other eye (dark blue shading). Axons from nasal retina target ventrolateral dLGN. Axons from the dLGN, in turn, project topographically onto V1. Axons from dorsomedial dLGN target the lateral region of V1 to generate the binocular segment (purple shading). Axons from ventrolateral dLGN target more medial, monocular parts of V1 (dark blue). This generates a single, cohesive topographic map of the right visual field in V1 of the left hemisphere. In Ten-m3 KO mice, ipsilateral axons (red) arise from the same region of retina as in WT mice but aberrantly target the entire ventrolateral extent of the dLGN. Thalamocortical mapping is not appreciably altered, thus, ipsilateral inputs, viewing central, binocular field, project not only to the lateral, normally binocular region of V1, but also target medial, normally monocular part of V1. Since thalamocortical topography is not altered, this area also receives input from peripheral visual field from the other eye. The expansion of ipsilateral input and misalignment of ipsilateral and contralateral inputs drives the formation of ipsilaterally and contralaterally dominated regions within layer 4 of V1.

Supplementary figure 1

Overlay of images showing distribution of c-fos immunoreactivity from all monocularly-inactivated KO and WT cases. Images were generated from tangential sections through layer 4 of ipsilateral V1, thresholded and artificially coloured, and normalized for mediolateral and rostrocaual variations in V1 size. In WT, signal was consistently confined to the lateral portion of V1 (n = 6). In contrast, in KO mice, thresholded signal was consistently in clusters that encroached into much more medial regions of V1 (n = 6).

Supplementary figure 2.

Preservation of contralateral retinotopy and aberrant ipsilateral drive in Ten-m3 KOs. Receptive fields of single units recorded from central V1 in Ten-m3 KO and WT mice. The contralateral receptive field is centred around 75 degrees eccentricity consistent with the retinotopic organisation recorded in WT mice. In two out of four cells, this region of visual space also received drive from the central, binocular field via the ipsilateral eye in Ten-m3 KOs. The ipsilateral and contralateral inputs are mismatched with respect to visual space. The WT cell did not receive ipsilateral drive above background levels.

Literature cited

1. Cang, J., Wang, L., Stryker, M.P. & Feldheim, D.A. Roles of ephrin-as and structured activity in the development of functional maps in the superior colliculus. *J Neurosci* **28**, 11015-11023 (2008).
2. Huberman, A.D., Feller, M.B. & Chapman, B. Mechanisms underlying development of visual maps and receptive fields. *Annu Rev Neurosci* **31**, 479-509 (2008).
3. Huberman, A.D., Speer, C.M. & Chapman, B. Spontaneous retinal activity mediates development of ocular dominance columns and binocular receptive fields in V1. *Neuron* **52**, 247-254 (2006).
4. Leamey, C.A., Van Wart, A. & Sur, M. Intrinsic patterning and experience-dependent mechanisms that generate eye-specific projections and binocular circuits in the visual pathway. *Curr Opin Neurobiol* **19**, 181-187 (2009).
5. Triplett, J.W.*, et al.* Retinal input instructs alignment of visual topographic maps. *Cell* **139**, 175-185 (2009).
6. Grubb, M.S., Rossi, F.M., Changeux, J.P. & Thompson, I.D. Abnormal functional organization in the dorsal lateral geniculate nucleus of mice lacking the beta 2 subunit of the nicotinic acetylcholine receptor. *Neuron* **40**, 1161-1172 (2003).
7. Malpeli, J.G. & Baker, F.H. The representation of the visual field in the lateral geniculate nucleus of Macaca mulatta. *J Comp Neurol* **161**, 569-594 (1975).
8. Reese, B.E. & Jeffery, G. Crossed and uncrossed visual topography in dorsal lateral geniculate nucleus of the pigmented rat. *J Neurophysiol* **49**, 877-885 (1983).
9. Hubel, D.H. & Wiesel, T.N. Receptive fields, binocular interaction and functional architecture in the cat's visual cortex. *J Physiol* **160**, 106-154 (1962).
10. Hubel, D.H. & Wiesel, T.N. Receptive fields and functional architecture of monkey striate cortex. *J Physiol* **195**, 215-243 (1968).
11. Hubel, D.H. & Wiesel, T.N. Laminar and columnar distribution of geniculo-cortical fibers in the macaque monkey. *J Comp Neurol* **146**, 421-450 (1972).
12. Shatz, C.J., Lindstrom, S. & Wiesel, T.N. The distribution of afferents representing the right and left eyes in the cat's visual cortex. *Brain Res* **131**, 103-116 (1977).
13. Wiesel, T.N., Hubel, D.H. & Lam, D.M. Autoradiographic demonstration of ocular-dominance columns in the monkey striate cortex by means of transneuronal transport. *Brain Res* **79**, 273-279 (1974).
14. Antonini, A., Fagiolini, M. & Stryker, M.P. Anatomical correlates of functional plasticity in mouse visual cortex. *J Neurosci* **19**, 4388-4406 (1999).
15. Drager, U.C. Receptive fields of single cells and topography in mouse visual cortex. *J Comp Neurol* **160**, 269-290 (1975).
16. Gordon, J.A. & Stryker, M.P. Experience-dependent plasticity of binocular responses in the primary visual cortex of the mouse. *J Neurosci* **16**, 3274-3286 (1996).
17. Fagiolini, M. & Hensch, T.K. Inhibitory threshold for critical-period activation in primary visual cortex. *Nature* **404**, 183-186 (2000).
18. Hubel, D.H., Wiesel, T.N. & LeVay, S. Plasticity of ocular dominance columns in monkey striate cortex. *Philos Trans R Soc Lond B Biol Sci* **278**, 377-409 (1977).
19. Kleinschmidt, A., Bear, M.F. & Singer, W. Blockade of "NMDA" receptors disrupts experience-dependent plasticity of kitten striate cortex. *Science* **238**, 355-358 (1987).

20. Leamey, C.A., *et al.* Ten_m3 regulates eye-specific patterning in the mammalian visual pathway and is required for binocular vision. *PLoS Biology* **5**, 2077-2092 (2007).
21. LeVay, S., Stryker, M.P. & Shatz, C.J. Ocular dominance columns and their development in layer IV of the cat's visual cortex: a quantitative study. *J Comp Neurol* **179**, 223-244 (1978).
22. Stryker, M.P. & Harris, W.A. Binocular impulse blockade prevents the formation of ocular dominance columns in cat visual cortex. *J Neurosci* **6**, 2117-2133 (1986).
23. Niell, C.M. & Stryker, M.P. Highly selective receptive fields in mouse visual cortex. *J Neurosci* **28**, 7520-7536 (2008).
24. Wang, Q. & Burkhalter, A. Area map of mouse visual cortex. *J Comp Neurol* **502**, 339-357 (2007).
25. Crair, M.C., Gillespie, D.C. & Stryker, M.P. The role of visual experience in the development of columns in cat visual cortex. *Science* **279**, 566-570 (1998).
26. Rakic, P. Prenatal genesis of connections subserving ocular dominance in the rhesus monkey. *Nature* **261**, 467-471 (1976).
27. Lowel, S. Ocular dominance column development: strabismus changes the spacing of adjacent columns in cat visual cortex. *J Neurosci* **14**, 7451-7468 (1994).
28. Boss, V.C. & Schmidt, J.T. Activity and the formation of ocular dominance patches in dually innervated tectum of goldfish. *J Neurosci* **4**, 2891-2905 (1984).
29. Cline, H.T., Debski, E.A. & Constantine-Paton, M. N-methyl-D-aspartate receptor antagonist desegregates eye-specific stripes. *Proc Natl Acad Sci U S A* **84**, 4342-4345 (1987).
30. Constantine-Paton, M. & Law, M.I. Eye-specific termination bands in tecta of three-eyed frogs. *Science* **202**, 639-641 (1978).
31. Schmidt, J.T. Retinal fibers alter tectal positional markers during the expansion of the retinal projection in goldfish. *J Comp Neurol* **177**, 279-295 (1978).
32. LeVay, S., Connolly, M., Houde, J. & Van Essen, D.C. The complete pattern of ocular dominance stripes in the striate cortex and visual field of the macaque monkey. *J Neurosci* **5**, 486-501 (1985).
33. Leamey, C.A., Protti, D.A. & Dreher, B. Comparative survey of the mammalian visual system with reference to the mouse. in *Eye, retina and visual system of the mouse* (ed. R.W. Williams & L.M. Chalupa) (MIT Press, Cambridge, MA, 2008).
34. Farley, B.J., Yu, H., Jin, D.Z. & Sur, M. Alteration of visual input results in a coordinated reorganization of multiple visual cortex maps. *J Neurosci* **27**, 10299-10310 (2007).
35. Yu, H., Farley, B.J., Jin, D.Z. & Sur, M. The coordinated mapping of visual space and response features in visual cortex. *Neuron* **47**, 267-280 (2005).
36. Toyoizumi, T. & Miller, K.D. Equalization of ocular dominance columns induced by an activity-dependent learning rule and the maturation of inhibition. *J. Neurosci.* **29**, 6514-6525 (2009).
37. Crowley, J.C. & Katz, L.C. Development of ocular dominance columns in the absence of retinal input. *Nat Neurosci* **2**, 1125-1130 (1999).
38. Crowley, J.C. & Katz, L.C. Early development of ocular dominance columns. *Science* **290**, 1321-1324 (2000).
39. Feng, K., *et al.* All four members of the Ten-m/Odz family of transmembrane proteins form dimers. *J Biol Chem* **277**, 26128-26135 (2002).

40. Oohashi, T., *et al.* Mouse ten-m/Odz is a new family of dimeric type II transmembrane proteins expressed in many tissues. *J Cell Biol* **145**, 563-577 (1999).
41. Leamey, C.A., *et al.* Differential Gene Expression between Sensory Neocortical Areas: Potential Roles for Ten_m3 and Bcl6 in Patterning Visual and Somatosensory Pathways. *Cereb Cortex* **18**, 53-66 (2008).
42. Li, H., Bishop, K.M. & O'Leary, D.D. Potential target genes of EMX2 include Odz/Ten-M and other gene families with implications for cortical patterning. *Mol Cell Neurosci* **33**, 136-149 (2006).
43. Bishop, K.M., Goudreau, G. & O'Leary, D.D. Regulation of area identity in the mammalian neocortex by Emx2 and Pax6. *Science* **288**, 344-349 (2000).
44. Hamasaki, T., Leingartner, A., Ringstedt, T. & O'Leary, D.D. EMX2 regulates sizes and positioning of the primary sensory and motor areas in neocortex by direct specification of cortical progenitors. *Neuron* **43**, 359-372 (2004).
45. Shatz, C.J. & LeVay, S. Siamese cat: altered connections of visual cortex. *Science* **204**, 328-330 (1979).
46. Guillery, R.W. An abnormal retinogeniculate projection in Siamese cats. *Brain Res* **14**, 739-741 (1969).
47. Guillery, R.W., Casagrande, V.A. & Oberdorfer, M.D. Congenitally abnormal vision in Siamese cats. *Nature* **252**, 195-199 (1974).
48. Kaas, J.H. & Guillery, R.W. The transfer of abnormal visual field representations from the dorsal lateral geniculate nucleus to the visual cortex in Siamese cats. *Brain Res* **59**, 61-95 (1973).
49. Kalatsky, V.A. & Stryker, M.P. New paradigm for optical imaging: temporally encoded maps of intrinsic signal. *Neuron* **38**, 529-545 (2003).

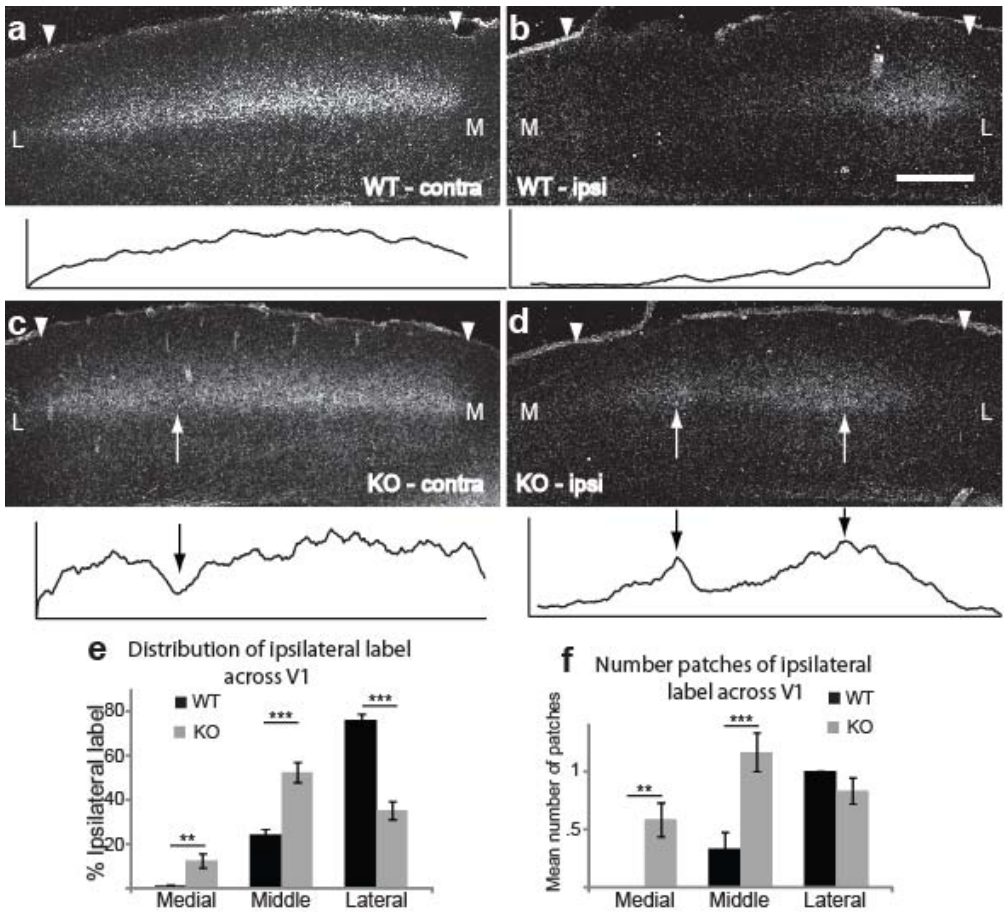
a
L
M
WT - contra
b
M
L
WT - ipsi
c
L
M
KO - contra
d
M
L
KO - ipsi
e
Distribution of ipsilateral label across V1
WT
KO
% Ipsilateral label
80
60
40
20
**
***
***
Medial
Middle
Lateral
f
Number patches of ipsilateral label across V1
WT
KO
Mean number of patches
1
.5
**
***
Medial
Middle
Lateral

Figure 1

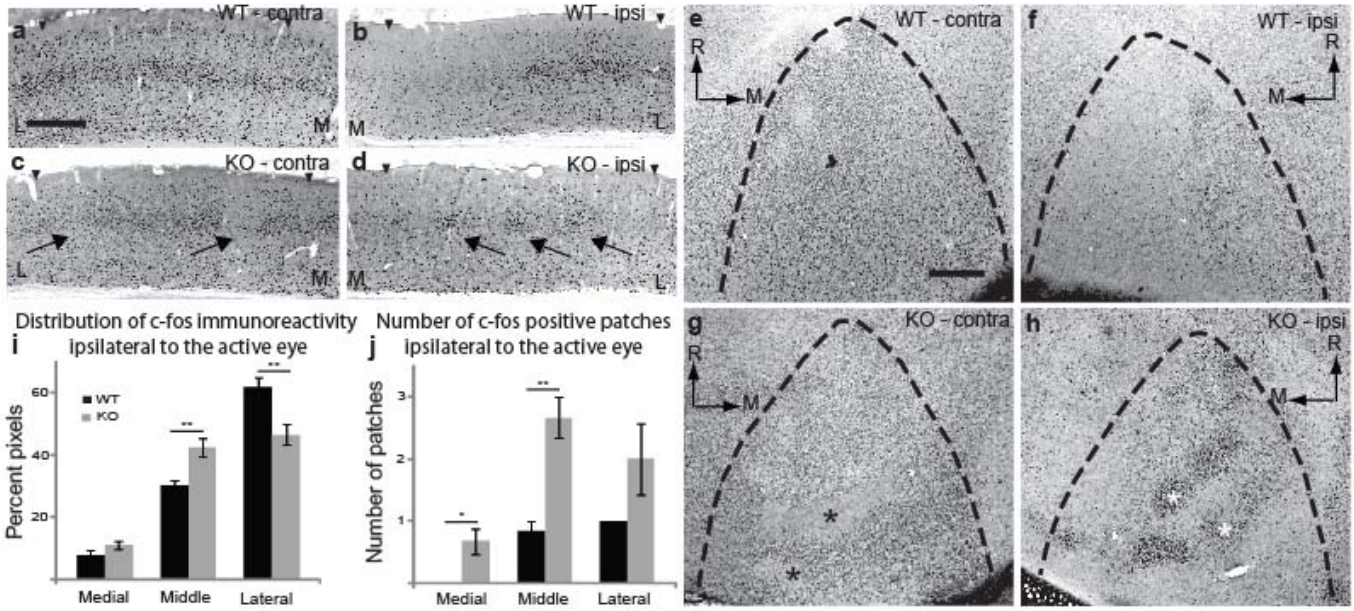
a
WT - contra
M
L
b
WT - ipsi
M
L
c
KO - contra
L
M
d
KO - ipsi
M
L
e
WT - contra
R
M
f
WT - ipsi
R
M
g
KO - contra
R
M
h
KO - ipsi
R
M
i
Distribution of c-fos immunoreactivity ipsilateral to the active eye
Percent pixels
WT
KO
Medial
Middle
Lateral
j
Number of c-fos positive patches ipsilateral to the active eye
Number of patches
Medial
Middle
Lateral

Figure 2

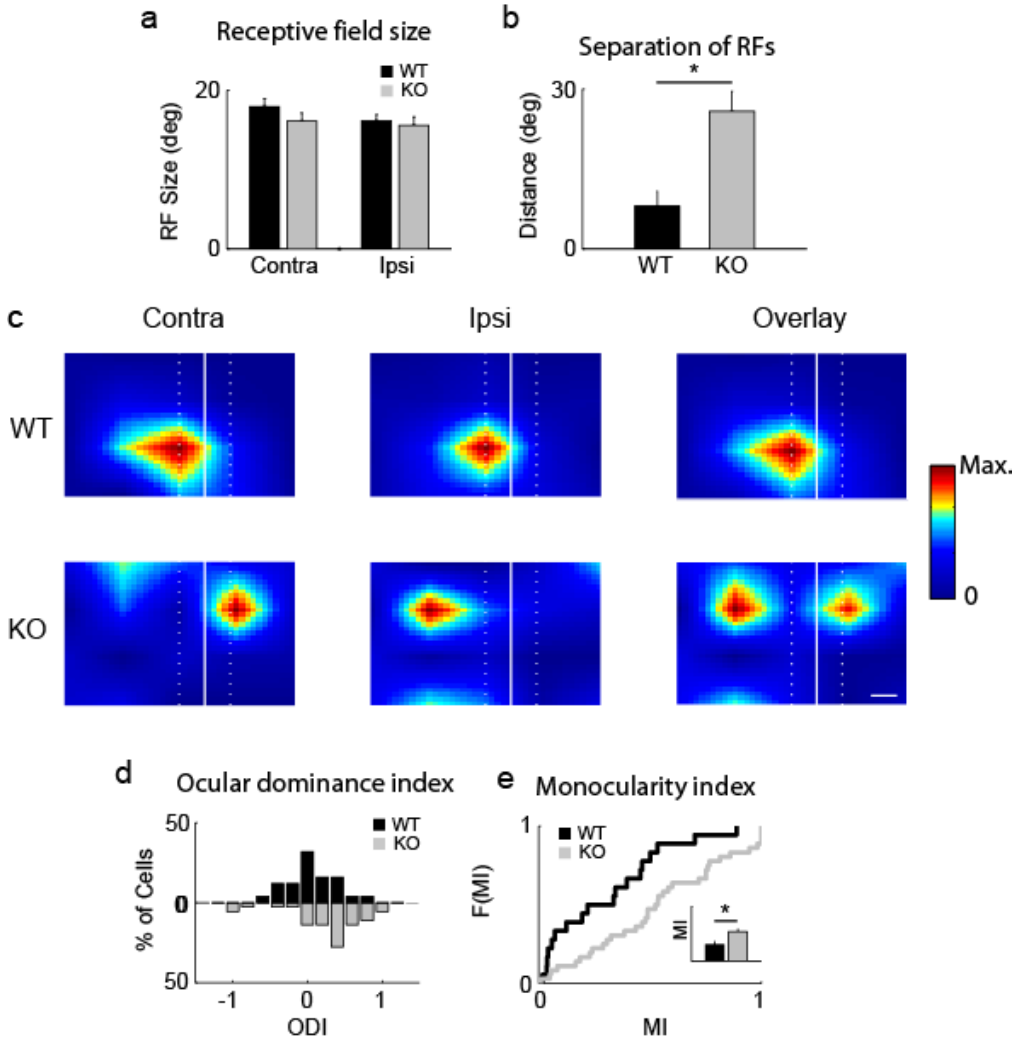
a
Receptive field size
WT
KO
RF Size (deg)
20
0
Contra
Ipsi
b
Separation of RFs
*
Distance (deg)
30
0
WT
KO
c
Contra
Ipsi
Overlay
WT
KO
Max.
0
d
Ocular dominance index
WT
KO
% of Cells
50
0
50
-1
0
1
ODI
e
Monocularity index
WT
KO
F(MI)
1
0
0
1
MI
MI
*

Figure 3

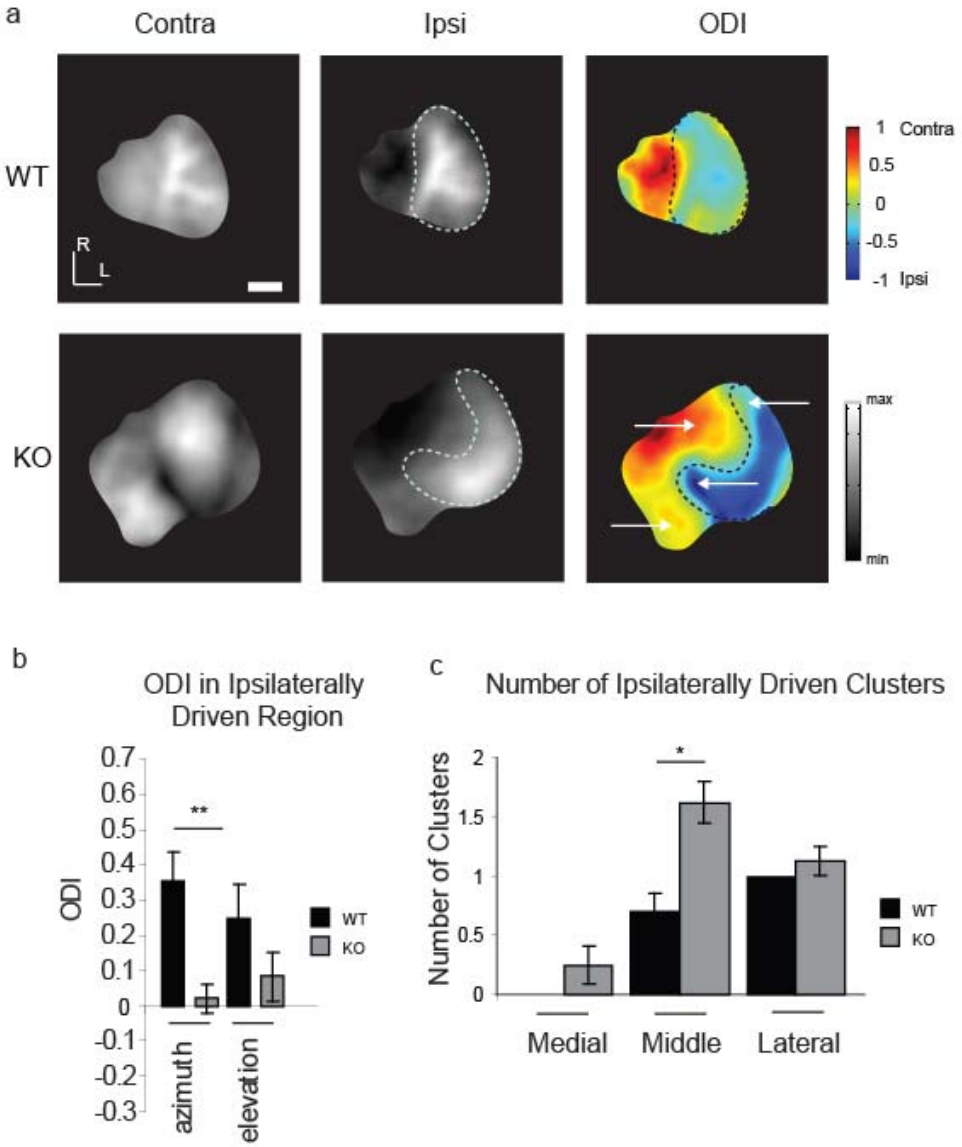
a
Contra
Ipsi
ODI
WT
KO
R
L
1 Contra
0.5
0
-0.5
-1 Ipsi
max
min
b
ODI in Ipsilaterally Driven Region
ODI
0.7
0.6
0.5
0.4
0.3
0.2
0.1
0
-0.1
-0.2
-0.3
**
azimuth
elevation
WT
KO
c
Number of Ipsilaterally Driven Clusters
Number of Clusters
2
1.5
1
0.5
0
*
Medial
Middle
Lateral
WT
KO

Figure 4

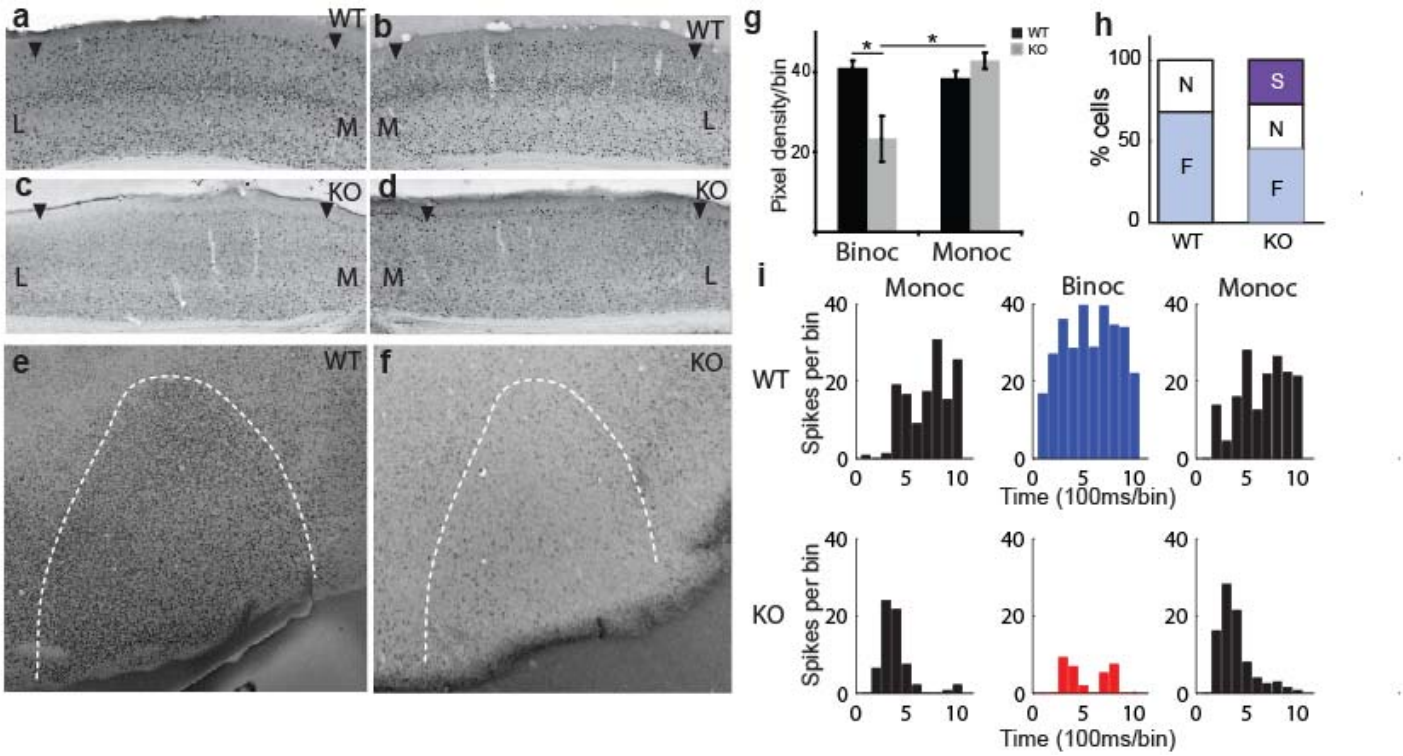
a
WT
L
M
b
WT
M
L
c
KO
L
M
d
KO
M
L
e
WT
f
KO
g
WT
KO
Pixel density/bin
40
20
*
*
Binoc
Monoc
h
% cells
100
50
0
N
F
S
N
F
WT
KO
i
Monoc
Binoc
Monoc
WT
KO
Spikes per bin
40
20
0
0
5
10
Time (100ms/bin)

Figure 5

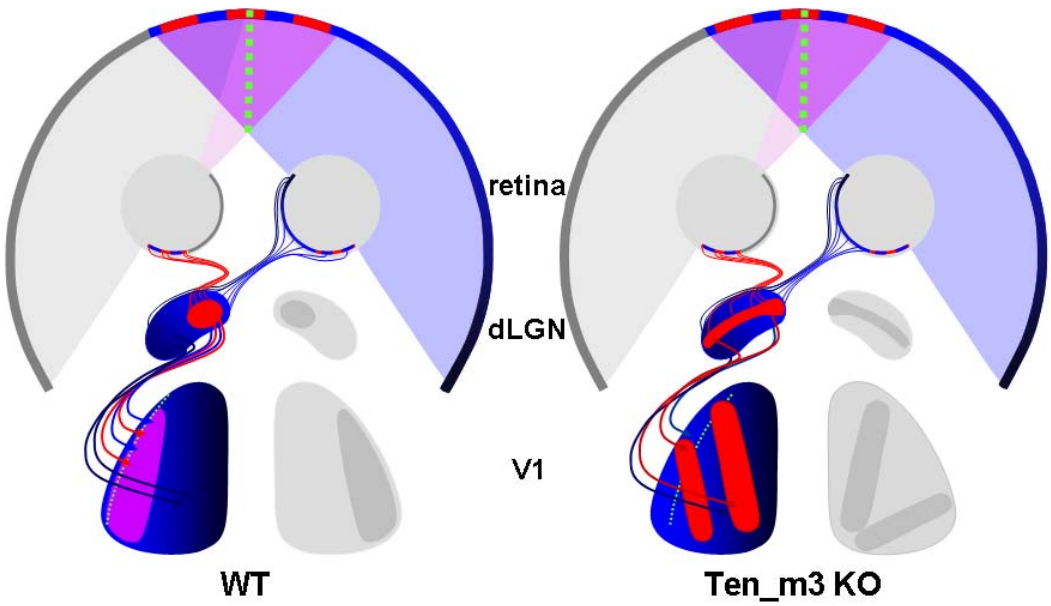

Figure 6

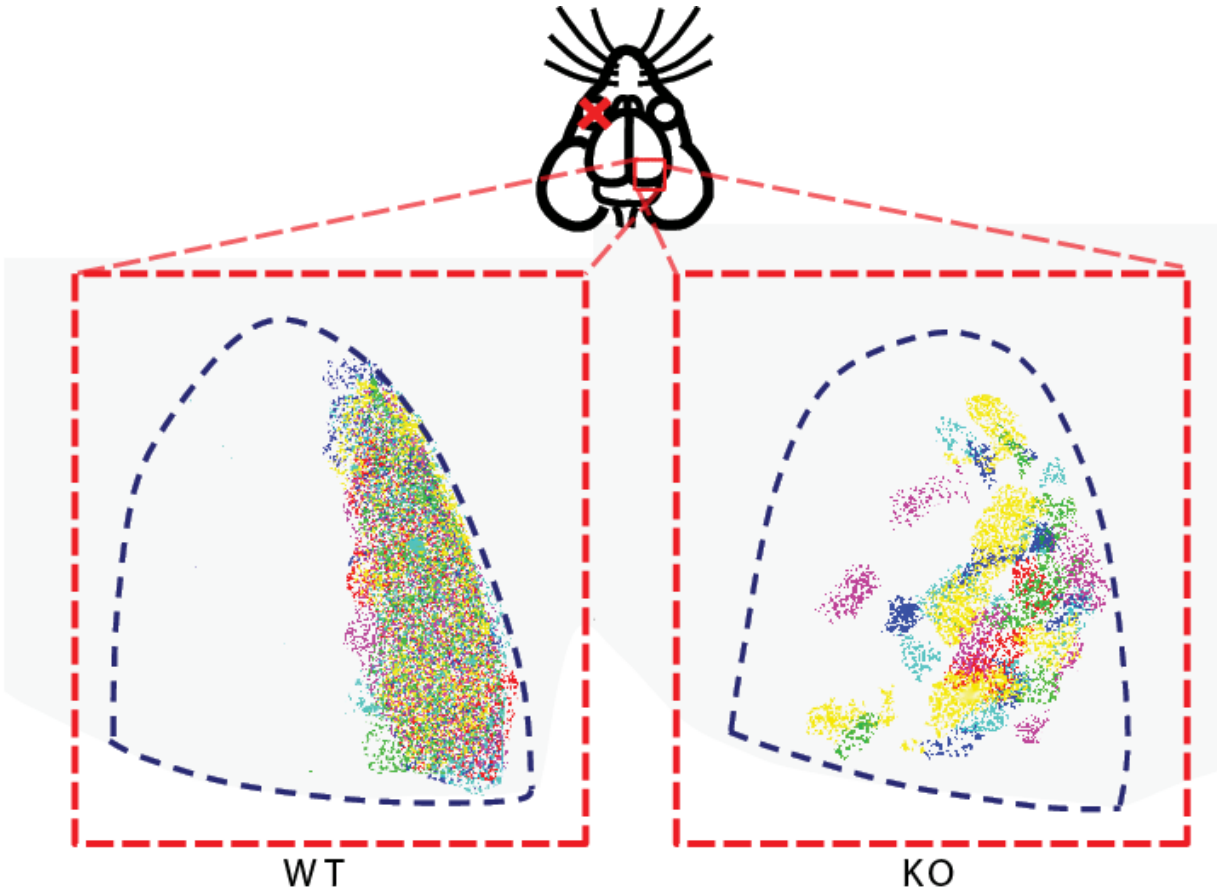

Supp figure 1:Overlay of images showing distribution of c-fos immunoreactivity from all monocularly-inactivated KO and WT cases. Images were generated from tangential sections through layer 4 of ipsilateral V1, thresholded and artificially coloured, and normalized for mediolateral and rostrocaual variations in V1 size. In WT, signal was consistently confined to the lateral portion of V1 (n = 6). In contrast, in KO mice, thresholded signal was consistently in clusters that encroached into much more medial regions of V1 (n = 6).

Merlin et al., supplementary figure 2

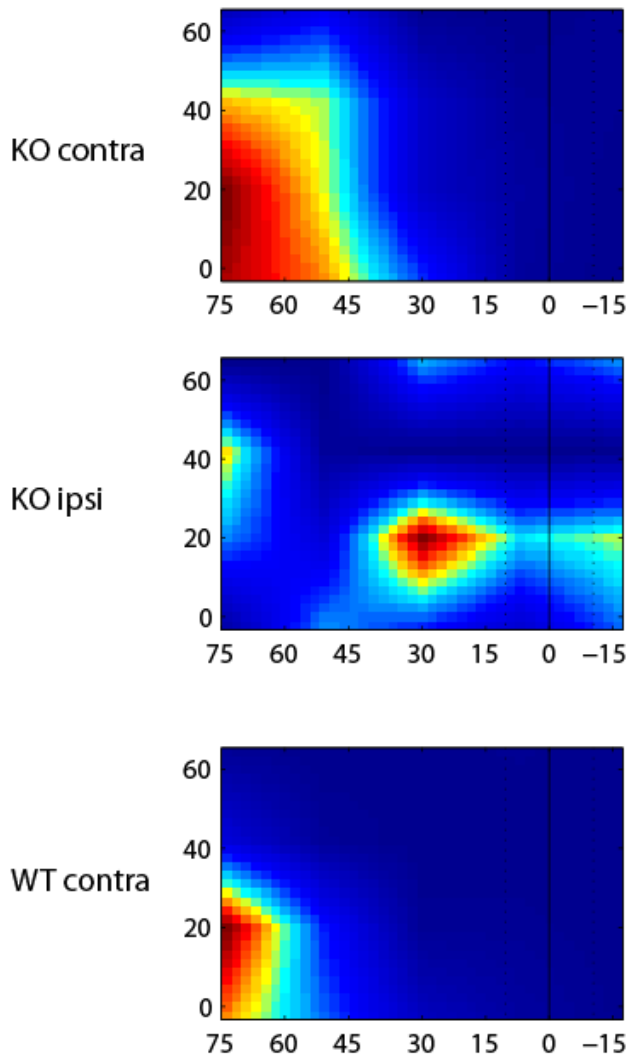

Supplementary figure 2. Preservation of contralateral retinotopy and aberrant ipsilateral drive in Ten-m3 KOs. Receptive fields of single units recorded from central V1 in Ten-m3 KO and WT mice. The contralateral receptive field is centred around 75 degrees eccentricity consistent with the retinotopic organisation recorded in WT mice. In two out of four cells, this region of visual space also received drive from the central, binocular field via the ipsilateral eye in Ten-m3 KOs. The ipsilateral and contralateral inputs are mismatched with respect to visual space. The WT cell did not receive ipsilateral drive above background levels.